HHS Public Access

Author manuscript

Nat Neurosci. Author manuscript; available in PMC 2016 August 22.

Published in final edited form as:

Nat Neurosci. 2016 April ; 19(4): 557–559. doi:10.1038/nn.4257.

Hyperactive Somatostatin Interneurons Contribute to Excitotoxicity in Neurodegenerative Disorders

Wen Zhang[#1], **Lifeng Zhang**[#1], **Bo Liang**[1], **David Schroeder**[2], **Zhong-wei Zhang**[2], **Gregory A. Cox**[2], **Yun Li**[1,4], and **Da-Ting Lin**[1,2,4]

[1]Intramural Research Program, National Institute on Drug Abuse, National Institutes of Health, 333 Cassell Drive, Baltimore, MD 21224, USA.

[2]The Jackson Laboratory, 600 Main Street, Bar Harbor, ME 04609, USA.

[#] These authors contributed equally to this work.

Abstract

Amyotrophic lateral sclerosis (ALS) and frontotemporal dementia (FTD) are overlapping neurodegenerative disorders whose pathogenesis remains largely unknown. Here using *TDP-43*^{A315T} mice, an ALS and FTD model with profound cortical pathology, we demonstrated that hyperactive somatostatin interneurons disinhibited layer 5 pyramidal neurons (L5-PN) and contributed to their excitotoxicity. Focal ablation of somatostatin interneurons efficiently restored normal excitability of L5-PN and alleviated neurodegeneration, suggesting a novel therapeutic target for ALS and FTD.

Amyotrophic Lateral Sclerosis (ALS) is a fatal neurodegenerative disorder characterized by progressive loss of motor neurons in both the motor cortex and the spinal cord [1–4]. Frontotemporal dementia (FTD) is a group of neurodegenerative disorders characterized by neuronal loss in the frontal and temporal cortices [5]. ALS and FTD share common genetic causes, including mutations in TAR DNA-binding protein 43 (*TDP-43*, gene symbol *Tardbp)* [6,7]. ALS and FTD also exhibit similar neuropathology with ubiquitinated protein inclusions containing TDP-43 [8], suggesting common pathological mechanisms [9,10]. The origin and progression of ALS and FTD remain largely unknown and curative therapies do not exist. Clinical neurophysiological studies of ALS patients indicate a potential involvement of dysfunctional cortical inhibition [11–15]. To explore the role of cortical inhibition in the pathogenesis of ALS and FTD, we examined neuronal functions in primary motor (M1)

[4]Correspondence to: Yun Li and Da-Ting Lin, **Contact Information**; Email: yunlijax@gmail.com and ; Email: lind3@mail.nih.gov

Author Contributions:

Y. Li, D. Lin, W. Zhang and L. Zhang designed the study and wrote the manuscript. W. Zhang and L. Zhang performed all the experiments and analysis. B. Liang helped with data analysis. D. Schroeder maintained some mouse colonies. G. Cox and Z. Zhang advised on experiments and manuscript preparation.

A supplementary methods checklist is available.

Competing Financial Interests Statement: The authors declare no competing financial interests.

cortex of *TDP-43*^{A315T} (*TDP*) mice, a transgenic mouse model recapitulating pathological aspects of ALS and FTD through over-expressing mutant human *TDP-43* gene [16].

To determine whether cortical inhibition is impaired in *TDP* mice, we first recorded miniature inhibitory postsynaptic currents (mIPSC) and evoked IPSC (eIPSC) from layer 5 pyramidal neurons (L5-PN), within M1 cortex of postnatal 3-week old *TDP* mice and their disease non-carrier littermates (WT). We found that both mIPSC and eIPSC were significantly reduced in *TDP* mice (**Fig. 1a, Supplementary Fig. 1a**). We also demonstrated that GABAergic synapse densities around somatic areas of L5-PN were significantly reduced in *TDP* mice (**Supplementary Fig. 1b**). In contrast, excitatory transmissions were similar in WT and *TDP* mice (**Supplementary Fig. 1c**).

L5-PN from 3-week old *TDP* mice exhibited hyperexcitability that was abolished by intracellular application of picrotoxin, a $GABA_A$ receptor blocker (Fig. 1b, Supplementary Fig. 1d, e, Supplementary Table 1). This observation suggests that hyperexcitability of L5-PN primarily originates from reduced GABAergic transmissions in *TDP* mice. The abnormalities in GABAergic transmission and L5-PN hyperexcitability in M1 cortex were sustained throughout disease progression in *TDP* mice (**Supplementary Fig. 2, Supplementary Table 2**).

To visualize excitotoxicity of L5-PN in *TDP* mice, we examined dendritic morphological changes, somatic cellular pathologies, and potential neurodegeneration of L5-PN at different disease stages. We found that dendritic blebs (an early sign of excitotoxicity [17]) appeared at early stage (Fig. 1c, Supplementary Fig. 3a-d, Supplementary Table 3), while profound ubiquitin positive aggregates and significant reduction of L5-PN appeared at the late disease stage of *TDP* mice (Fig. 1d, Supplementary Fig. 3e, Supplementary Table 4). Together, our data suggest that sustained impairments in GABAergic transmission of L5-PN lead to its hyperexcitability, excitotoxicity, and neurodegeneration in *TDP* mice.

To identify the origin of impaired GABAergic transmission in *TDP* mice, we first examined intrinsic activities of somatostatin (Sst) and parvalbumin (Pv) expressing interneurons, the two major interneuron populations in the mouse cortex [18]. In postnatal 3-week old *TDP* mice, Sst interneurons were hyperactive, while Pv interneurons were hypoactive, with significantly increased spontaneous IPSCs (sIPSCs) but normal mIPSCs (**Fig. 2a-c, Supplementary Fig. 4a**). Importantly, Sst interneurons continued to be hyperactive in adult *TDP* mice and their numbers increased at the late stage of *TDP* mice (**Fig. 2d, Supplementary Fig. 5)**. In contrast, Pv interneurons in adult *TDP* mice appeared normal (**Supplementary Fig. 4b-d**). Sst interneurons inhibit Pv interneurons in mouse visual cortex [19], and disinhibit layer 4 excitatory neurons in somatosensory cortex [20]. We therefore propose a pathogenic mechanism in *TDP* mice, where dysfunctional Sst interneurons serve as the primary driving force for the excitotoxicity of L5-PN: hyperactive Sst interneurons disinhibit L5-PN and lead to its hyperexcitibility through inhibition of Pv interneurons.

To illustrate the potential disinhibition connectivity between Sst interneurons and L5-PN in M1 cortex, we performed whole-field optogenetic stimulations to either activate or inactivate Sst interneurons and measured the excitability of L5-PN. We found that activation of Sst

interneurons increased while inhibition of Sst interneurons decreased the firing frequency of L5-PN (**Supplementary Fig. 6a-c**). We further confirmed that Sst interneurons disinhibited L5-PN *via* modulating GABAergic inputs to L5-PN, by demonstrating that activation of Sst interneurons decreased while inactivation of Sst interneuron increased charge transfer of sIPSCs in L5-PN (**Fig. 2e, Supplementary Fig. 6d**). In contrast, Pv interneurons directly inhibited L5-PN (**Supplementary Fig. 6e**).

To directly test the hypothesis that sustained hyperactive Sst interneurons cause excitotoxicity of L5-PN in *TDP* mice, we next asked if eliminating Sst interneurons in early adulthood of *TDP* mice would restore normal excitability of L5-PN, and rescue cortical neuropathology and neurodegeneration **(Supplementary Fig. 7)**. We genetically labeled Sst interneurons with diphtheria toxin receptor (DTR) and injected diphtheria toxin (DT) locally to bilaterally ablate Sst interneurons in M1 cortex at 6-week old mice (**Supplementary Fig. 8**). Two weeks following Sst interneuron ablation in *TDP* mice, we found a significant increase in the frequency of mIPSCs of L5-PN (**Fig. 3a**). Loose-seal cell-attached recordings of L5-PN demonstrated that Sst interneuron ablation in *TDP* mice fully restored the spiking activity of L5-PN to levels similar to those of disease non-carrier controls (**Fig. 3b**). In separate groups of *TDP* mice following six weeks bilateral DT injection, we found that Sst interneuron ablation in *TDP* mice significantly increased GABAergic synaptic density on L5-PN, reduced ubiquitin positive aggregates in M1 cortex, and reversed the neuronal loss in M1 cortex of *TDP* mice (**Fig. 3c-e**). Together, these results support our hypothesis that the excitotoxicity of L5-PN is primarily driven by sustained hyperactive Sst interneurons in M1 cortex of *TDP* mice.

In sum, we discovered a specific microcircuit between Sst interneurons and L5-PN in M1 cortex where Sst interneurons send an overall disinhibitory signal to L5-PN *via* inhibiting Pv interneurons. Most importantly, we demonstrated that in *TDP* mice, this inhibitory neuronal circuit was dysfunctional and therefore contributed to the cortical pathogenesis in ALS and FTD. We propose targeting this subpopulation of inhibitory interneurons as a novel therapeutic concept for ALS and FTD.

Online Methods

Mice

All experiments were conducted in accordance with procedures established by the Administrative Panels on Laboratory Animal Care at The Jackson Laboratory and NIH. Transgenic mice used in this manuscript were: B6.Cg-*Tg(Prnp-TARDBP*A315T)95Balo*/J (010700, *TDP-43*^{A315T} or *TDP*); B6.Cg-*Tg (Thy1-YFPH)2Jrs*/J (003782, *Thy1-YFPH* or *YFP*); B6.Cg-*Gt(ROSA)26Sor*$^{tm14(CAG-tdTomato)Hze}$/J (007914, *tdTomato*); STOCK *Sst*$^{tm2.1(cre)Zjh}$/J (013044, *SstCre* or *Sst*); B6.Cg-*Pvalb*$^{tm1.1(cre)Aibs}$/J (012358, *PvCre* or *Pv*); C57BL/6-*Gt(ROSA)26Sor*$^{tm1(HBEGF)Awai}$/J (007900, *DTR*). Male mice were used across the studies.

Slice Preparation

Male mice age P20-22, P50-60, and P90-100 were euthanized with CO_2 and decapitated. 250 μm coronal slices were prepared with a vibratome (Leica VT1000 S and VT1200) in ice-cold cutting solution contained the following (in mM): 80 NaCl, 26 $NaHCO_3$, 3.0 KCl, 1.0 NaH_2PO_4, 1.3 $MgCl_2$, 1.0 $CaCl_2$, 20 D-glucose, and 75 sucrose, saturated with 95% O_2 and 5% CO_2. Slices were then moved to an incubation chamber containing artificial cerebrospinal fluid (ACSF) contained the following (in mM): 124 NaCl, 26 $NaHCO_3$, 3.0 KCl, 1.0 NaH_2PO_4, 1.3 $MgCl_2$, 1.5 $CaCl_2$, 20 D-glucose, saturated with 95% O_2 and 5% CO_2). Sliced were incubated first at 34°C for 30 minutes and then at room temperature (21°C) until used for recordings.

Electrophysiological recordings

L5-PN in M1 cortex was identified by cell morphology and size, and recorded using methods as previously described [21]. Brain slices were placed in a submersion type chamber continuously perfused with ACSF saturated with 95% O_2 and 5% CO_2 at 32 – 33°C.

For IPSC recordings, the pipette solution contained the following (in mM): 120 CsCl, 4 ATP-Mg, 0.3 GTP, 0.5 EGTA, 10 HEPES, and 4.0 QX-314 (pH 7.2, 270–280 mOsm with sucrose). Miniature IPSC recordings were performed in the presence of 20 μM DNQX, 50 μM AP5, and 1 μM tetrotoxin (TTX). For recordings of evoked IPSC, a concentric bipolar electrode (FHC) was placed in L5 of M1 cortex at a fixed distance of 200 μm to the recorded cell to apply stimuli.

For EPSC recordings, the pipette solution contained (in mM): 110 Cs methylsulfate, 15 CsCl, 4 ATP-Mg, 0.3 GTP, 0.5 EGTA, 10 HEPES, and 4.0 QX-314 (pH 7.2, 270–280 mOsm with sucrose). Miniature EPSC (mEPSC) was recorded in the presence of 1 μM TTX and 100 μM picrotoxin.

Electrodes had resistances between 2 and 3.5 MΩ. The series resistance was not compensated in voltage-clamp experiments. During experiments, the series resistance was constantly monitored. Data were discarded when series resistance was >16 MΩ or change of series resistance was >15%.

For current-clamp recording, the pipette solution contained (in mM): 120 K-gluconate, 10 KCl, 4 ATP-Mg, 0.3 GTP, 10 HEPES, and 0.5 EGTA (pH 7.2, 270–280 mOsm with sucrose). Series resistance was fully compensated using the bridge circuit of the amplifier MultiClamp 700B. Action potential threshold was estimated as the point when the slope of rising membrane potential exceeds 50 mV ms^{-1}.

For photo-stimulation of ChR2 and eNpHR3.0, we used a high-power light source (HXP 120V, Zeiss) controlled by AxoGraph X with TTL signal. Light was delivered onto brain slices through a band-pass filter (470-740 nm for ChR2, 605-670 nm for eNpHR3.0) *via* a 40×objective (NA 0.8).

For loose-seal cell-attached recordings of L5-PN, the electrodes were filled with ACSF and a loose patch of > 50 MΩ was achieved for recording with the bath application of 20 mM KCl.

Recordings were performed with Multiclamp 700B (Molecular Devices). Experiments were conducted using AxoGraph X (AxoGraph Scientific). Data were filtered at 4 kHz and digitized at 20 kHz. Data were analyzed offline using Axograph X and Igor Pro (Wavemetrics).

Cranial window preparation and two-photon imaging acquisition

We crossed *TDP-43^{A315T}* (*TDP*) mice with *Thy1-YFPH* mice in which L5-PN are fluorescence labeled with YFP, and using their disease non-carrier fluorescent littermates as controls. We performed surgery to generate non-invasive "thin-skulled" cranial window, with a relative larger optical window (1 mm in diameter) compared to the traditional preparation procedure (200 μm in diameter) [22,23]. Thin-skulled cranial window requires repeatable thinning prior image acquisition due to the skull regeneration. We obtained *in vivo* images twice for one particular mouse. To generate a thin-skulled cranial window, experimental mice (at age of 6-weeks) were anesthetized and the cranial sutures from the bregma to lambda were exposed. Under a dissecting microscope, a high-speed micro-drill was used to thin and polish a circular region (~ 1 mm diameter) in the skull over the motor cortex to a final thickness of 15-20 μm. This circle was centered on the right hemisphere (AP: +1.2 mm, ML: +2.0 mm), to ensure that the optical window is above the motor cortex region [24]. A glass coverslip (1 mm square, #1 thickness) was fused to the thinned skull with a layer of cyanoacrylate cement, and the skull was sealed with dental cement [23]. See also **Supplementary Fig. 3**.

Neuronal morphology was acquired using a custom two-photon microscope operated using custom software (ScanImage). Fine vascular patterns observed through the cranial window were used as landmarks to enable repeated imaging of the same group of neurons. We obtained the initial *in vivo* two-photon images of L5-PN two days after the surgery day. At the age of 9-weeks or 15-weeks we re-thinned the original cranial window and obtained the repetitive images.

Morphology and size are the two main criteria to identify "blebs". The morphology of blebs is unique as "beads on a string", which is very different from regular dendritic spine. We initially identified "blebs" manually based on the morphology. And the size of L5-PN dendritic blebbings was quantified, and the number of dendritic blebbings was quantified and normalized with corresponding image areas across groups. We found that the size of blebs was much bigger than that of spines. A spine is in general less than 1 μm^2 (area), while a bleb is in an average of ~ 12.8μm^2 (ranging from 2.7μm^2 to 64 μm^2). We also counted blebs "semi-automatically": first set up a threshold of 3 μm^2 to automatically identify potential blebs; then manually exclude the false counts resulting from dendritic intersections. These two methods gave us similar results. We only presented the data analysis from manual identification.

Immunostaining

Mice were anesthetized with ketamine and xylazine (100 mg kg^{-1} and 10 mg kg^{-1}, respectively). For VGAT and Pv staining, mice were perfused with phosphate-buffer saline (PBS, pH 7.4) and then 4% paraformaldehyde (PFA) in PBS. Brain tissues were post-fixed

with 4% PFA in PBS overnight at 4 °C, and 40μm coronal sections were prepared with vibratome. VGAT and Pv immunostaining followed the standard protocols for free-floating sections. In brief, free-floating sections were incubated in blocking solution containing 4% normal goat serum, 1% bovine serum albumin (BSA), and 0.3% triton X-100 in PBS, with slowly shaking for 2 hours at room temperature. Sections were then treated with primary antibody in blocking solution for overnight at 4 °C and with secondary antibody in blocking solution at room temperature for 2 hours with slowly shaking. Stacked images (4μm each stack) were obtained through Leica Confocal Microscopy.

For ubiquitin staining, mice were perfused with PBS and then Bouin's solution. Brain tissues were post-fixed in Bouin's solution overnight at 4 °C and submitted blindly to the Jackson Laboratory Histology Core to be processed for paraffin embedding and ubiquitin staining. Sst immunostaining with paraffin embedded sections was similar procedure except that the sections were deparaffinized and went through the antigen retrieval step (microwave boiling for 9 minutes in 0.01M citrate, pH = 6.0).

Primary antibodies used were mouse anti-parvalbumin [25] (1:1000 dilution, p3088, Sigma-Aldrich, St. Louis, MO), rabbit anti-VGAT [21] (1:2000 dilution, 131003, Synaptic Systems, Germany), rabbit anti-somatostatin [26] (1:300 dilution, sc-13099, Santa Cruz Biotechnology, Santa Cruz, CA), mouse anti-NeuN [27] (1:1000 dilution, ab104224, Abcam, Cambridge, MA) and mouse anti-ubiquitin [28] (1:500 dilution, 3936, Cell Signaling Technology, Beverly, MA). Secondary antibodies used were Alexa Fluor 647 donkey anti-mouse IgG [29] (1:300 dilution, 715-605-150, Jackson ImmunoResearch Laboratories, West Grove, PA) and Alexa Fluor 647 donkey anti-rabbit IgG [30] (1:300 dilution, 711-605-152, Jackson ImmunoResearch Laboratories).

ImageJ software was used for VGAT puncta density analysis from brain slices of *YFP* and *TDP::YFP* mice with VGAT immunostaining. YFP signal was used to outline somatic area of L5-PN. VGAT puncta inside the somatic outline were quantified through Particle Analysis with parameters of 0.1 ~ 4μm in size and 0.1 ~ 1.00 in circularity. Custom script in MATLAB was used to calculate the density of VGAT puncta from brain slices of VGAT and NeuN co-immunostaining. Briefly, VGAT signals with intensity three times above the standard deviation of the image background were detected. The NeuN signal was used to define the region of interest (ROI). Only ROIs within layer 5 and with a minimal area of 300 μm^2 were identified as presumably L5-PN and pursued for further analysis. VGAT puncta for each identified ROI was quantified with a spot-detection algorithm.

For NeuN positive cell count, images of layer 5 in M1 cortex were taken with a confocal microscope (Zeiss LSM 710) equipped with a 40x objective (NA 1.3), then NeuN positive cell density was calculated by dividing cell number by the image area (212.55 μm × 212.55 μm).

Injection of AAV virus for ChR2, eNpHR3.0, or eYFP expression

Adeno-associated viruses (AAV1) for Cre dependent expression of ChR2, eNpHR3.0, and eYFP were acquired from the University of Pennsylvania Viral Vector Core: pAAV1-EF1a-DIO-hChR2(H134R)-eYFP-WPRE-pA (titer 3.4×10^{12} genome copies each milliliter),

pAAV1-EF1a-DIO-eNpHR3.0-eYFP-WPRE-pA (titer 7×10^{12} genome copies each milliliter), and pAAV1-EF1a-DIO-eYFP-WPREohGH (titer 1.8×10^{13} genome copies each milliliter). To perform optogenetic experiments, Cre dependent ChR2 or eNpHR3.0 viruses were 1:5 diluted with saline and injected into M1 cortex region (AP: +1.5 mm, ML: +2.0 mm) of postnatal 6-7 weeks of *PvCre* and *SstCre* mice at a depth of 1.25 mm using a micropump (WPI). A total of 300 nanoliter of virus was injected over 5 min. To identify Sst and Pv interneurons in adulthood *TDP* mice, Cre dependent eYFP virus were 1:5 diluted with saline and injected into the M1 cortex of postnatal 6-7 weeks of *PvCre*, *TDP::PvCre*, *SstCre*, and *TDP::SstCre* mice. Two weeks after virus injection mice were sacrificed for electrophysiology experiments.

Toxin injection

6-weeks old mice were anesthetized with 2 - 2.5 % isoflurane for diphtheria toxin (DT) injection, placed on a heating pad maintained at 37°C. 0.5 μl of DT (100 pg μl^{-1} in saline) was stereotaxically injected bilaterally into the M1 cortex region (AP: +1.2 mm, ML: ±2.0 mm, DV: −1.6mm) at 0.1 μl min^{-1}, using a 10 μl syringe (Hamilton Company) connected to a microsyringe pump controller (World Precision Instruments).

Sample size, randomization and blinding statement

Sample sizes for electrophysiological recordings and for *in vivo* imaging and immunostainings were estimated based on past experience and those presented in the literature. Typically, recordings of $n > 10$ neurons from at least 3mice each group were collected for electrophysiological studies; $n > 10$ images from at least 5 mice each group were collected for in vivo imaging; and $n > 10$ counts from each side of slices from at least 3 mice each group were collected for immunostaining.

Mice were randomly allocated to treatment condition and all data were randomly collected.

Initial electrophysiological recordings (*i.e.,* mIPSCs), Ubiquitin stainings, NeuN immunostainings, and VGAT immunostainings were performed in a blinded manner. All other data were collected and analyzed without the investigator blinded to genotype and treatment conditions.

Statistical analysis

All statistical comparisons were performed with two-sided tests. For comparisons between two groups, D'Agostino & Pearson omnibus test was used for normality test and the variances were calculated with Prism5.0 analysis function. If both groups displayed normal distributions and had equal variance, unpaired t-test was used; otherwise non-parametric Mann-Whitney *U*-test was used. For comparisons between multiple groups, Jarque-Bera test was used for normality test, and Levene's test was used for variance test. If all groups have normal distribution and equal variance, one-way ANOVA with *post-hoc* Tukey test was used. If multiple groups exhibited different variances, Brown and Forsythe Test with *post-hoc* Games-Howell test were used. In these tests, data distribution was assumed to be normal but this was not formally tested. For experiment with photoactivation of ChR2 and eNpHR3.0, Wilcoxon signed rank test and paired t-test were used (Jarque-Bera test was used

for normality test, and Levene's test was used for variance test). $P < 0.05$ was accepted as statistically significant.

Code availability

Custom script in MATLAB, which was used for VGAT puncta density analysis, is available upon request.

Supplementary Material

Refer to Web version on PubMed Central for supplementary material.

Acknowledgements

Research was supported by Jackson Lab Startup Funds (DTL), 1R21 NS075382-01A1 (YL and GAC), and the Intramural Research Program of the National Institute on Drug Abuse (DTL).

References

1. Vucic S, Kiernan MC. Curr Mol Med. 2009; 9:255–272. [PubMed: 19355908]
2. Ravits JM, La Spada AR. Neurology. 2009; 73:805–811. [PubMed: 19738176]
3. Rothstein JD. Ann Neurol. 2009; 65(Suppl 1):S3–9. [PubMed: 19191304]
4. Perry JJ, Shin DS, Tainer JA. Adv Exp Med Biol. 2010; 685:9–20. [PubMed: 20687491]
5. Seeley WW. Curr Opin Neurol. 2008; 21:701–707. [PubMed: 18989116]
6. Kabashi E, et al. Nat Genet. 2008; 40:572–574. [PubMed: 18372902]
7. Sreedharan J, et al. Science. 2008; 319:1668–1672. [PubMed: 18309045]
8. Neumann M, et al. Science. 2006; 314:130–133. [PubMed: 17023659]
9. Baloh RH. Curr Opin Neurol. 2012; 25:701–707. [PubMed: 23041957]
10. Ling SC, Polymenidou M, Cleveland DW. Neuron. 2013; 79:416–438. [PubMed: 23931993]
11. Enterzari-Taher M, Eisen A, Stewart H, Nakajima M. Muscle Nerve. 1997; 20:65–71. [PubMed: 8995585]
12. Ziemann U, et al. Neurology. 1997; 49:1292–1298. [PubMed: 9371911]
13. Zanette G, et al. J Neurol. 2002; 249:1723–1728. [PubMed: 12529797]
14. Karandreas N, et al. Amyotroph Lateral Scler. 2007; 8:112–118. [PubMed: 17453640]
15. Vucic S, Nicholson GA, Kiernan MC. Brain. 2008; 131:1540–1550. [PubMed: 18469020]
16. Wegorzewska I, Bell S, Cairns NJ, Miller TM, Baloh RH. Proc Natl Acad Sci U S A. 2009; 106:18809–18814. [PubMed: 19833869]
17. Lin RC, Matesic DF, Connor JA. Ann N Y Acad Sci. 1997; 825:134–145. [PubMed: 9369982]
18. Kubota Y. Curr Opin Neurobiol. 2014; 26:7–14. [PubMed: 24650498]
19. Pfeffer CK, Xue M, He M, Huang ZJ, Scanziani M. Nat Neurosci. 2013; 16:1068–1076. [PubMed: 23817549]
20. Xu H, Jeong HY, Tremblay R, Rudy B. Neuron. 2013; 77:155–167. [PubMed: 23312523]
21. Zhang W, Peterson M, Beyer B, Frankel WN, Zhang ZW. Loss of MeCP2 from forebrain excitatory neurons leads to cortical hyperexcitation and seizures. The Journal of neuroscience : the official journal of the Society for Neuroscience. 2014; 34:2754–2763. [PubMed: 24523563]
22. Yang G, Pan F, Parkhurst CN, Grutzendler J, Gan WB. Thinned-skull cranial window technique for long-term imaging of the cortex in live mice. Nat Protoc. 2010; 5:201–208. [PubMed: 20134419]
23. Zhang LF, et al. Imaging glioma initiation in vivo through a polished and reinforced thin-skull cranial window. J. Vis. Exp. 2012 DOI: 10.3791/4201.
24. Pronichev IV, Lenkov DN. Functional mapping of the motor cortex of the white mouse by a microstimulation method. Neurosci Behav Physiol. 1998; 28:80–85. [PubMed: 9513982]

25. Tricoire L, et al. A blueprint for the spatiotemporal origins of mouse hippocampal interneuron diversity. The Journal of neuroscience : the official journal of the Society for Neuroscience. 2011; 31:10948–10970. [PubMed: 21795545]

26. Nakamura M, et al. Signaling complex formation of phospholipase Cbeta4 with metabotropic glutamate receptor type 1alpha and 1,4,5-trisphosphate receptor at the perisynapse and endoplasmic reticulum in the mouse brain. The European journal of neuroscience. 2004; 20:2929–2944. [PubMed: 15579147]

27. Kaur P, Karolina DS, Sepramaniam S, Armugam A, Jeyaseelan K. Expression profiling of RNA transcripts during neuronal maturation and ischemic injury. PloS one. 2014; 9:e103525. [PubMed: 25061880]

28. Stum M, et al. An assessment of mechanisms underlying peripheral axonal degeneration caused by aminoacyl-tRNA synthetase mutations. Molecular and cellular neurosciences. 2011; 46:432–443. [PubMed: 21115117]

29. Huckleberry KA, et al. Behavioral experience induces zif268 expression in mature granule cells but suppresses its expression in immature granule cells. Frontiers in systems neuroscience. 2015; 9:118. [PubMed: 26347620]

30. Teixeira FK, et al. ATP synthase promotes germ cell differentiation independent of oxidative phosphorylation. Nature cell biology. 2015; 17:689–696. [PubMed: 25915123]

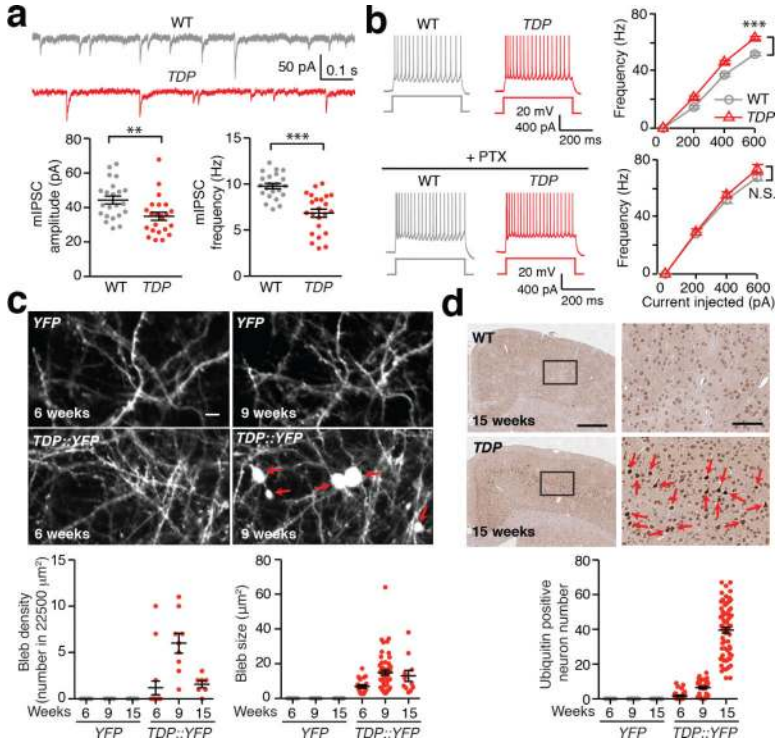

Figure 1. Reduced GABAergic transmission, hyperexcitability, and excitotoxicity of L5-PN in *TDP* mice

(**a**) L5-PN in *TDP* mice (3-week age) exhibited reduced mIPSC. Top: representative mIPSC traces. Bottom: dot plots of amplitude and frequency of mIPSC (WT and *TDP*, n = 22, 23 neurons, 3 mice; Mann-Whitney *U*-test). (**b**) L5-PN in *TDP* mice (3-week age) exhibited hyperexcitability, originated from changes in inhibitory transmission. Left: representative action potential (AP) responses to 400 pA current injection. Right: frequency-current (F-I) plots in the absence and presence of 350 μM PTX (WT and *TDP*, n = 53, 58 neurons, 6 mice; with PTX application, n = 40, 50 neurons, 3 mice; Mann-Whitney *U*-test). (**c**) Dendritic blebbing occurred in *TDP::YFP* mice. Top: representative *in vivo* images (red arrows indicated blebs; scale bar, 5 μm). Bottom: dot plots of density and size of blebs (*YFP* and *TDP::YFP*, n = 18, 9, 9 and 16, 9, 7 images, 10, 5, 5 mice across groups). (**d**) Ubiquitin pathology in M1 cortex of *TDP* mice. Top: representative cortical images (scale bar, 500 μm) and high magnifications from boxed areas (red arrows indicated ubiquitin positive neurons; scale bar, 100 μm). Bottom: dot plots of ubiquitin positive neuron numbers (n = 18, 42, 54 counts from 9, 21, 27 slices, 3, 4, 3 WT mice; and n = 42, 36, 72 counts from 21, 18, 36 slices, 4, 3, 6 *TDP* mice across groups). Error bars are mean ± SEM. *, $p < 0.05$; **, $p < 0.01$; ***, $p < 0.001$; N.S., not significant.

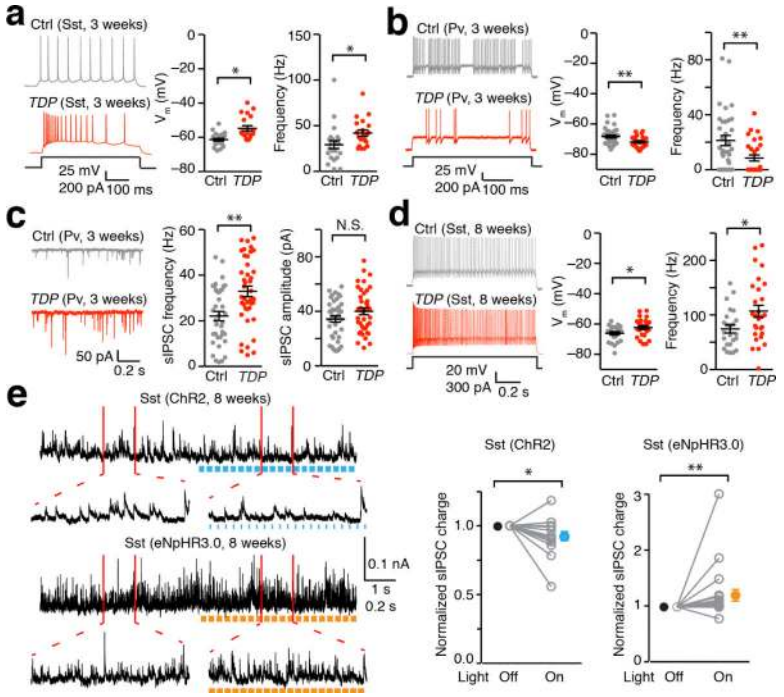

Figure 2. Hyperactive Sst neurons lead to sustained disinhibition of L5-PN in *TDP* mice

(**a**) Hyperactive Sst interneurons in M1 cortex of 3-week old *TDP* mice. Left: representative AP firings of Sst interneurons in response to 200 pA current injection, from *SstCre::tdTomato* (Ctrl) and *TDP::SstCre::tdTomato* (*TDP*) mice. Right: dot plots of resting membrane potential (RMP) and AP firing frequency (Ctrl and *TDP*, n = 23, 20 neurons, 3 mice; Mann-Whitney *U*-test). (**b**) Hypoactive Pv interneurons in M1 of 3-weeks old *TDP* mice. Left: representative AP firings of Pv interneurons in response to 200 pA current injection, from *PvCre::tdTomato* (Ctrl) and *TDP::PvCre::tdTomato* (*TDP*) mice. Right: dot plots of RMP and AP firing frequency (Ctrl and *TDP*, n = 34 and 29 neurons, 3 mice; Mann-Whitney *U*-test). (**c**) Pv interneurons exhibited increased frequency of sIPSC in 3-week *TDP* mice. Left: representative sIPSC traces from *PvCre* (Ctrl) and *TDP::PvCre* (*TDP*) mice injected with Cre dependent eYFP virus. Right: dot plots of frequency and amplitude of sIPSC (Ctrl and *TDP*, n = 39, 41 neurons, 3 mice; Mann-Whitney *U*-test). (**d**) Sustained hyperactive Sst interneurons in M1 cortex of 8-week old *TDP* mice. Left: representative AP firings of Sst interneurons in response to 300 pA current injection, from *SstCre* (Ctrl) and *TDP::SstCre* (*TDP*) mice injected with Cre dependent eYFP virus. Right: dot plots of RMP and AP firing frequency (Ctrl and *TDP*, n = 24, 28 neurons, 3 mice; Mann-Whitney *U*-test). (**e**) Photo-stimulation of ChR2 (10 ms, 20 Hz) and eNpHR3.0 (40 ms, 20 Hz) on Sst interneurons of M1 cortex induced changes in sIPSCs of L5-PN. Left: representative sIPSC traces of L5-PN before and after photo-stimulation of Sst interneurons, from 8-week old *SstCre* mice injected with Cre dependent ChR2 or eNpHR3.0 virus. Right: Population (open circles) and average (filled circles) of normalized ratio ("light on" over "light off") in sIPSC charges of ChR2 and eNpHR3.0 (n = 15, 20 neurons, 3 mice; Wilcoxon Signed Rank Test). Error bars are mean ± SEM. *, $p < 0.05$; **, $p < 0.01$; N.S., not significant.

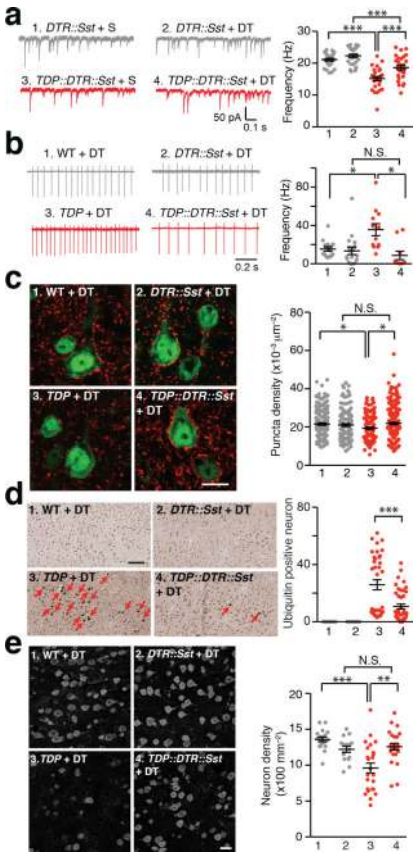

Figure 3. Bilateral ablation of Sst interneurons diminished excitotoxicity of L5-PN in *TDP* mice

(**a**) Two-week bilateral ablation of Sst interneurons in M1 cortex of *TDP* mice increased L5-PN mIPSC frequency. Left: representative traces of L5-PN mIPSCs. Right: dot plots of the frequencies of mIPSCs (S, saline; Group 1 to 4, n = 25, 26, 27, 28 neurons, 3 mice; One-way ANOVA and *post hoc* Tukey test). (**b**) Two-week bilateral ablation of Sst interneurons in M1 restored normal excitability of L5-PN in *TDP* mice. Left: representative traces of AP firing of L5-PN, through loose-seal cell-attached recordings with bath-application of 20 mM KCl. Right: dot plots of AP firing frequencies (Group 1 to 4, n = 15, 18, 12, 10 neurons, 3, 4, 4, 3 mice; Brown and Forsythe Test and *post hoc* Games-Howell test). (**c**) Six-week bilateral ablation of Sst interneurons in M1 cortex of *TDP* mice increased vesicular GABA transporter (VGAT) punta in L5-PN. Left: representative images of VGAT staining (Red, VGAT; Green, NeuN; scale bar, 10 μm). Right: dot plots of puncta densities (Group 1 to 4, n = 180, 120, 143, 195 neurons, 3, 2, 3, 3 mice; Brown and Forsythe test and *post hoc* Games-Howell test). (**d**) Six-week bilateral ablation of Sst interneurons reduced ubiquitin positive aggregates in *TDP* mice. Left: representative images (red arrows indicated ubiquitin positive neurons; scale bar, 100 μm). Right: dot plots of ubiquitin positive neuron numbers (Group 1 to 4, n = 24, 24, 36, 42 counts, from 12, 12, 18, 21 slices of 4, 4, 6, 7 mice; Mann-Whitney *U*-test). (**e**) Six-week bilateral ablation of Sst interneurons reversed neuronal loss in M1 cortex of *TDP* mice. Left: representative images of NeuN immunostaining (scale bar, 20 μm). Right: dot plots of layer 5 neuron densities (Group 1 to 4, n = 18, 16, 24, 24 counts from 9, 8, 12, 12 slices of 3, 3, 4, 4 mice; Brown and Forsythe test and *post hoc* Games-

Howell test). Error bars are mean ± SEM. *, $p < 0.05$; **, $p < 0.01$; ***, $p < 0.001$; N.S., not significant.